Characterization Of Biaxial Strain Of Poly(L-Lactide) Tubes

Løvdal, Alexandra Liv Vest; Andreasen, Jens Wenzel; Mikkelsen, Lars Pilgaard; Agersted, Karsten; Almdal, Kristoffer

Published in:
Polymer International

Link to article, DOI:
10.1002/pi.5040

Publication date:
2016

Document Version
Peer reviewed version

Characterization Of Biaxial Strain Of Poly(L-Lactide) Tubes

Authors: **Alexandra Løvdal[1], Jens W Andreasen[2], Lars P Mikkelsen[3], Karsten Agersted[2], Kristoffer Almdal[1]**

[1]Technical University of Denmark, Department of Micro- and Nanotechnology. [2]Technical University of Denmark, Department of Energy Conversion and Storage.[3]Technical University of Denmark, Department of Wind Energy.

Address: *Technical University of Denmark, Department of Micro- and Nanotechnology*, Ørsteds Plads, 345E, 2800 Kongens Lyngby, Denmark.

Corresponding author: A Løvdal, alvlo@nanotech.dtu.dk

Keywords: Poly(L-lactide), strain-induced crystallinity, biaxial strain, WAXS

Abstract

Poly(L-lactide) (PLLA) in its L-form has promising mechanical properties. Being a semi-crystalline polymer, it can be subjected to strain-induced crystallization at temperatures above T_g and can thereby become oriented. Following a simultaneous (SIM) biaxial strain process or a sequential (SEQ) biaxial strain process, the mechanical properties of biaxial strained tubes can be further improved. This study investigated these properties in relation to their morphology and crystal orientation. Both processes yield the same mechanical strength and modulus, yet exhibit different crystal orientation. Through further WAXS analysis it was found that the SEQ biaxial strain yields larger interplanar spacing and distorted crystals and looser packing of chains. However, this does not influence the mechanical properties negatively. A loss of orientation in SEQ biaxial strained samples at high degrees of strain was detected, but not seen for SIM biaxial strain, and did not correlate with mechanical performance in either case. However, post-annealing reduced the orientation to the same level in both cases, and the modulus and strength is decreased for both SIM and SEQ biaxial. It is therefore concluded that mechanical properties after biaxial strain are related to strain-induced amorphous orientation and the packing of crystals, rather than strain-induced crystallinity.

Introduction

Poly(L-lactide) (PLLA) is a biodegradable and bioabsorbable semi-crystalline aliphatic polyester, which can be derived from starch based products. It has been of interest as a replacement for petrolbased polyesters in both the packaging industry and in the biomedical industry.[1-4] It has its drawback in lack of sufficient mechanical and physical barrier properties.[5] Both the physical and mechanical properties strongly depend on the structure of the polymer, including the crystal morphology.[6] In its L-lactic form, PLLA, it has promising mechanical properties, which can be

improved further by crystallization. Isothermal (ISO) crystallization has been done to improve the properties for PLLA, but is often done at high annealing temperature and/or durations unfavorable for production in the industry.[7-9] Deformation of PLLA in its amorphous form at temperatures above glass transition temperature (T_g) and below cold crystallization temperature (T_{cc}) have been widely investigated in relation to its crystallinity, orientation of the molecular chains within the amorphous regions.[8,10-15] The deformation stimulates the otherwise slow crystallization kinetics for PLLA at lower temperatures, observed during cold crystallization or from melt.[13,16] It thereby increases stiffness and strength related to a rise in crystallization.[17] Several studies on mechanical properties during deformation have been performed on PLLA film, which was strained or deformed at a given degree of strain, rate and/or temperature, although little was revealed about the mechanical properties remaining after deformation. [2,6,10,11-13,14,18-21] Because film fabrication is a common process in the industry, and is done to improve mechanical properties, groups have investigated both uniaxially and biaxially strained films.[12,22,23] The objective of this study is to investigate the changes in crystallinity, crystal size and orientation of crystals and the amorphous chains and discussing in relation to the mechanical properties (elastic modulus and yield stress). Additionally, the objective is to identify how the process, whether simultaneous (SIM) or sequential (SEQ) biaxial strain, influences the orientation and crystal size in comparison to ISO crystallization.

Experimental

PLLA 2003D pellets were purchased from NatureWorks LLC (Minnetonka, MN, USA) (~4.1 % D-isomer; molecular weight, 1.85 x 10^5 g/mol), heated to 194 °C and extruded into small tubes with an outer diameter of 3.4 mm and an inner diameter of 1.7 mm. After extrusion, the tubes were quenched well below T_g in a cooling medium at 15.5 °C for 14.5 s, leaving the tube with low crystallinity (~1%), as determined by differential scanning calorimetry (DSC).

Expansion process

The extruded tubes were expanded to different diameters using a custom-made setup. Prior to expansion, a section of the extruded tubes was heated in a cylindrical form at 100 °C. The heating time determines the inner tube temperature and, in this case, 73 °C was aimed for. The total expansion degree is dependent on axial strain as well as the radial strain. The expansion process in this paper is regarded as biaxial straining and was done either simultaneously (SIM) or sequentially (SEQ). For comparison, tubes strained uniaxially (UNI) along the axial direction were processed. Figure 1 portrays a sketch of the raw material, after axial elongation and radial expansion.

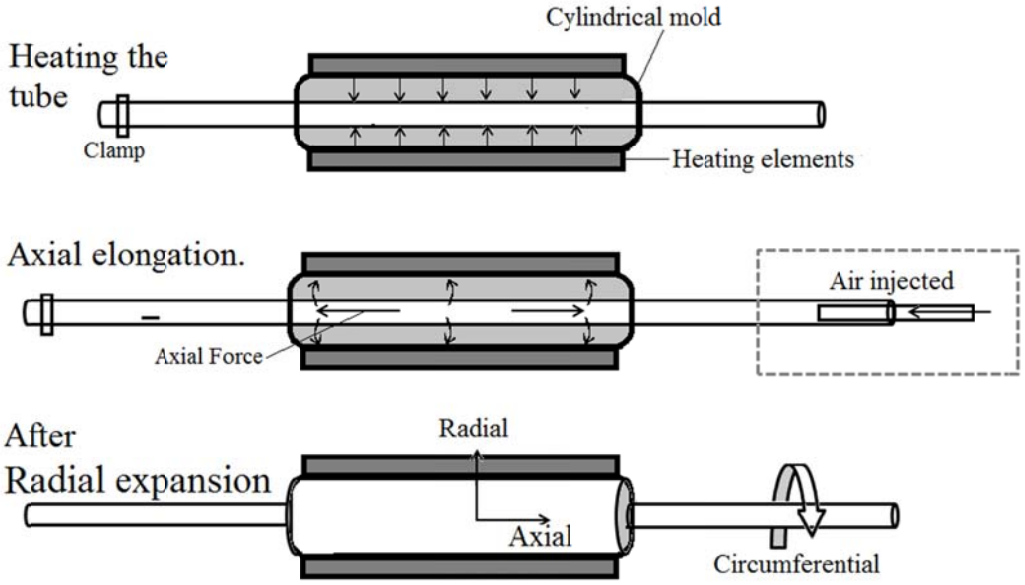

Figure 1 Sketch of biaxial straining. The extruded tube is placed in a cylindrical mold of a given diameter with heating elements surrounding the mold.

Once heat transfer to the inner lumen of the tube has taken place for the specified amount of time the tube is elongated by application of an axial force. If pressure is applied prior to axial elongation by injection of air into the tube lumen, the tube is expanded radially into the shape and size of the

mold as the elongation occurs. This process is described as simultaneous (SIM) biaxial strain. If the pressure is applied after the elongation the process is described as sequential (SEQ) biaxial strain.

SIM biaxial strain

An internal pressure was created by injecting air inside the lumen of the tube prior to heating. Once heated, the tube was axially elongated with the speed of 100 mm/s to the desired length. The tube expands to the given form size at the instant it is pulled axially.

SEQ biaxial strain

After heating, the tube was axially stretched from each end to a desired length, after which the pressure was applied and the tube was expanded to the given form size.

The axial strain (ε_a) is given for each specimen as the change in length (ΔL) over the original length (L_0) (Eq. 1). The radial strain (ε_r) is given as the change in diameter (ΔR) over the diameter prior to axial strain (R_0) minus the reduction in thickness due to the axial strain (t_a) (Eq. 2).

$$\boldsymbol{\varepsilon_a} = \frac{\boldsymbol{\Delta L}}{\boldsymbol{L_0}} \quad \text{Eq. 1}$$

$$\boldsymbol{\varepsilon_r} = \frac{\boldsymbol{\Delta R}}{\boldsymbol{R_0 - t_a}} \quad \text{Eq. 2}$$

Total area expansion (A_{exp}), or the degree of expansion, is the relation between the radius after any axial strain and the radius after expansion (R_2) (Eq. 3). The radius after axial (R_1) strain is calculated with the assumption that the volume of the material is the same before and after axial strain (see Eq. 4).

$$\boldsymbol{A_{exp}} = \frac{\boldsymbol{R_2}}{\boldsymbol{R_1}} \cdot \mathbf{100}\% \quad \text{Eq. 3}$$

$$\boldsymbol{R_1} = \sqrt{\frac{{R_0}^2 \cdot L}{(L+\Delta L)}} \quad \text{Eq. 4}$$

Specimen preparation

Specimens for circumferential testing were cut as rings with a width (*w)* of 5 mm and a length (*L)* of 18 mm. Specimens for axial testing were cut as strips along the tube with the same dimensions. The cross sectional area was determined as the average thickness of each ring and strip times the width of the specimens.

Mechanical testing

Uniaxial tensile testing was performed in both the axial and circumferential direction using a tensile tester (Instron 5564) at a testing speed of 2.7 mm/min, corresponding to a strain rate of 0.15 min^{-1}. and pulled to fracture. Data obtained from mechanical testing represents the normal strain and stress values. From the data, the elastic modulus (E) was found in the stress interval of 20-40 MPa. The yield stress (σ_y) was determined as local maximum before strain hardening begins.

Wide angle X-ray scattering (WAXS)

Orientation and crystallinity changes were evaluated by wide angle X-ray scattering (WAXS). Samples were examined using a custom made 2D diffraction setup equipped with a rotating anode Cu Kα X-ray source, monochromated and focused by 1D multilayer optics (λ=1.5418 Å), operated at 50 kV and 200 mA as described in Apitz et al, 2005.[24] The tube sample was cut in half and placed perpendicular to the beam. Distance between detector and sample was 123 mm.

Measurement duration was 30 min. The crystalline interplanar spacings (d) were determined from Bragg's law (Eq. 5):

$$\boldsymbol{d} = \frac{\boldsymbol{\lambda}}{\boldsymbol{2 \cdot \sin\theta}} \quad \text{(Eq. 3)}$$

The degree of orientation was found using Herman's orientation function (Eq.6), and second order orientation factor (Eq. 7), as described in further detail by Sakurai et al, 2001,[25] quantifies the orientation of the lamellae in the stretching direction. The scattering intensity on the 2D detector is integrated as a function of radial angle 2θ, and as a function of azimuthal angle ϕ, with ϕ = 0° defined at the position of the axial and circumferential directions according to the maximum intensity for the reflections corresponding to the 110 planes. The intensity *(I (ϕ))* corresponding to diffraction from the 110/200 planes was integrated in the interval of scattering vectors q = 1.13-1.24 Å^{-1} between 0-360^{o} azimuthal angle. The orientation is defined according to the symmetry axes of the diffraction pattern. Total orientation has been achieved when F2 is one, and random orientation when F2 is zero. $\langle cos^2\phi \rangle$ is the average of $cos^2\phi$.

$$\boldsymbol{f_H} = \frac{\boldsymbol{3\langle \cos^2 \phi \rangle - 1}}{\boldsymbol{2}} \quad \text{(Eq. 6)}$$

$$\langle \cos^2 \phi \rangle = \frac{\int_0^{\pi} I(\phi) \cos^2\phi \sin\phi \, d\phi}{\int_0^{\pi} I(\phi) \sin\phi \, d\phi}$$

$$\boldsymbol{F_2} = \boldsymbol{-2 \cdot f_H} \quad \text{(Eq. 7)}$$

The mean crystal size (D) normal to a particular reflection plane (hkl) was found by Scherrer's equation (Eq. 8) using K as a dimensionless shape factor set to 0.9 [25], λ as the X-ray wavelength (1.5418 Å) and $\beta_{½}$ as the full-width at half maximum of the peak at Bragg diffraction angle, θ.

$$D_{(hkl)} = \frac{K \cdot \lambda}{\beta_{½} \cos\theta} \quad \text{(Eq. 8)}$$

Crystal size in the circumferential direction (D_c) was determined from the peak in the scattering vector (q) interval of 2.2-2.25 $Å^{-1}$ corresponding to (018) plane[26], whereas crystal size in the axial direction (D_a) was found for the planes (110/200) in the scattering vector interval of 1.13-1.24 $Å^{-1}$.

Thermal properties of PLLA tubes were analysed using a differential scanning calorimeter (NETZSCH DSC 200 F3 Maia). Samples of 5-10 mg were heated (10 °C/min) from 0 °C to 200 °C in a nitrogen atmosphere (50 ml/min). Data analysis was done in NETZSCH Proteus Analysis software v6.1. The T_g was found as the midline between onset and offset of the transition. The degree of crystallinity (X_c) was calculated from the enthalpy induced by melting (ΔH_m) minus the heat fusion induced by cold crystallization (ΔH_c) relative to the enthalpy of fusion (ΔH°) of a 100 % crystalline PLLA sample[27] (Eq. 9). For PLLA ΔH° is set to 93 J/g.[28]

$$X_c(\%) = \frac{(\Delta H_m - \Delta H_c)}{\Delta H^\circ} \cdot 100\% \quad \text{(Eq. 9)}$$

Enthalpies were quantified through determination of the respective areas for which borders were related to extrapolated on-sets and off-sets of the individual traces. The reproducibility of determinations for runs on consecutive identical samples is 0.06 % crystallinity. The uncertainty for one particular curve of fitting the area of the melting peak is almost one order of magnitude better. Runs on different samples from the same lot, i.e. from different positions in the reactor resulted in a variation of about 2 %, which is an expression of inhomogeneity.

For comparison between ISO crystallization and strain-induced crystallinity, heating of an extruded tube at 90 °C for 60 min was done, having an X_c= 30 %. Additionally, the effect of annealing at 90 °C for 60 min on strained tubes, both SIM and SEQ biaxial strain, was determined with DSC.

Results

Mechanical testing

Stress/strain curves in the circumferential direction portray the typical behaviour of a semi-crystalline polymer in the sense that the specimen is strain-hardening as it undergoes elongation (see Figure 2a and b). Elongation at rupture improve with degree of axial strain, when keeping the radial strain constant. The strain hardening effect is not detected in the axial direction (see Figure 3), which shows a maximum stress value before 10 % strain. At the same time, the slope of the strain hardening region becomes steeper with A_{exp}. In general, more variation was detected for samples with a high degree of strain (1.0;3.2 in Figure 2a and b), yet a larger fracture strength was detected when increasing the strain both axially and radially. Unlike the circumferential specimens, elongation at fracture in the axial direction varies and did not occur over the entire gauge length, but failed in localized area.

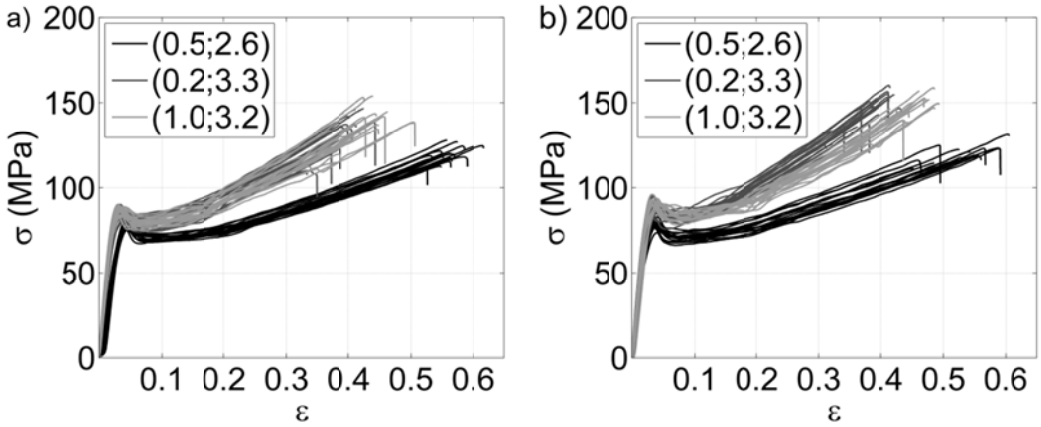

Figure 2 Stress (σ)/strain (ε) curves for SIM (a) and SEQ (b) biaxially strained tubes in the circumferential direction. The axial and radial strains are given in parentheses separated by semicolon (ε_a; ε_r).

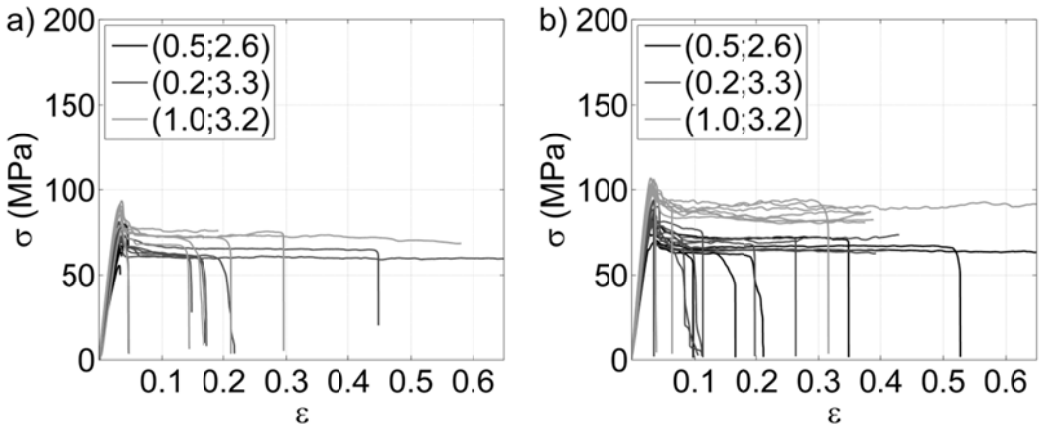

Figure 3 Stress (σ)/strain (ε) curves for SIM (a) and SEQ (b) biaxially strained tubes in the axial direction.

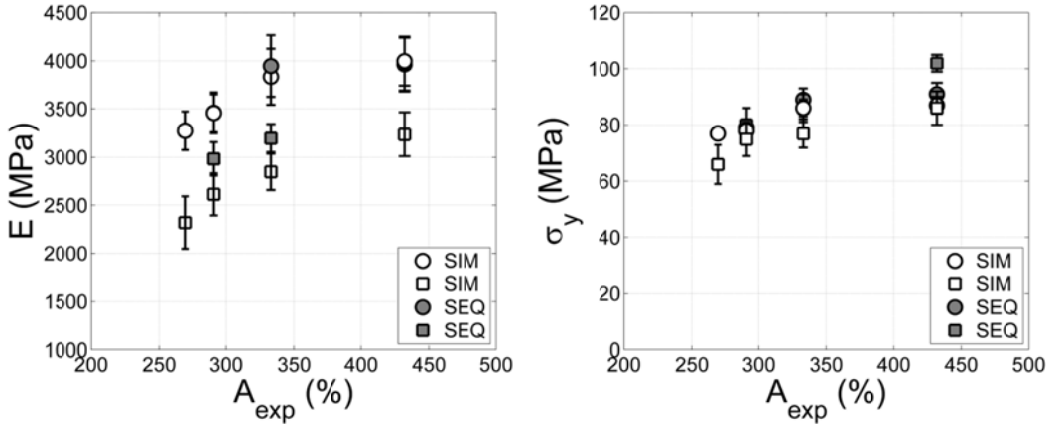

Figure 4 Elastic modulus ($E_{20\text{-}40}$) and yield stress (σ_y) of Poly(L-lactide) (PLLA) tubes obtained from tensile testing in both circumferential (○) and axial (□) directions as a function of A_{exp}.

The elastic moduli in both the circumferential as well as the axial direction increase with A_{exp} (Figure 4). Velazquez-Infante et al, 2012,[17] tested thin films of PLLA with similar D-isomer content

and found similar values for elastic modulus (3.7-3.9 GPa) and yield stress (56.2-60.2 MPa), and the strain-induced crystallization seen in oriented film applies for tubes as well. Sequential straining does not affect the axial modulus as much as the simultaneous does. Simultaneously strained sample show a larger degree of anisotropic behaviour in the two directions than the sequentially strained samples. The yield stress increases with degree of strain in both directions, regardless of processing method. The yield stress in the axial direction for SEQ biaxially strained samples, showed higher values than SIM. This means that the orientation of chains (crystal formation or not) during the axial elongation has a larger influence on the strength of the material rather than the modulus of the material.

Creating a SIM biaxially strained material by applying a transverse strain to uniaxial strainleads to destruction of crystallites (decrease in their size) with poor crystalline regions[11,12]. During a SEQ strain, the transverse strain will gradually destroy the crystalline structure obtained in the uniaxial direction; it also creates a crystalline structure in the transverse direction. One could expect destruction of crystals formed uniaxially and new ones formed transversely would create a larger anisotropy in the material for SEQ as opposed to SIM biaxial strain. However, in this specific case the mechanical properties of both SIM and SEQ biaxially strained samples appear to have the same degree of isotropy within the material.

Crystallinity

The UNI (1.0;0) allows formation of the highest X_c of 34 %, and subsequent heating allows a formation of 36 % crystallinity (Table 2). The SEQ and SIM biaxially strained samples showed overall no difference in DSC scans (see Figure 5) and the same crystallinity of 29-32 %. UNI with axial strain at 0.2 and 0.5 did not induce any crystallinity.

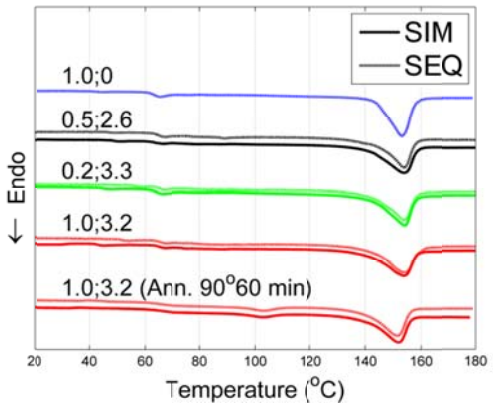

Figure 5 DSC heating curves of PLLA strained either UNI strain, SIM or SEQ biaxially strained tubes with or without post-annealing at 90 °C for 60 min.

The T_g does not change significantly as a function of area expansion for SEQ biaxial straining, however there is a slight increase in T_g for SIM biaxial strain. During heating of the SEQ and SIM biaxial samples for 60 min at 90 °C, no exothermal crystallization appear, despite the crystallinity being far from the maximum X_c of PLLA, which has been reported at 57 % after annealing at 160 °C for 10 hours[29] but can go as high as 65 % after straining.[18] Therefore the biaxially strained tubes are unable to crystallize further at this temperature. The results showed that the X_c is independent of the ratio between axial and radial strain and remains constant, which is not in agreement with Chen et al, 2011.[27]

From other thermal measurements (not listed here), it is seen that the strain-induced crystallinity forms at strains close to 100 % and above. The crystalline phase is thereby oriented in the strain direction. When the strain applied is large enough, some crystals are destroyed while new crystals are formed. The X_c after deformation depends on the amount of new crystals formed and the amount that are destroyed. Destroying the crystals will decrease the crystallinity. A decrease in crystallinity at higher strains may also be caused by formation of cavitation. The decrease seen for

the expanded tubes is about 3 %; this decrease was also observed by Zhang et al, 2011,[28] who proved existence of voids or cavitations.

WAXS

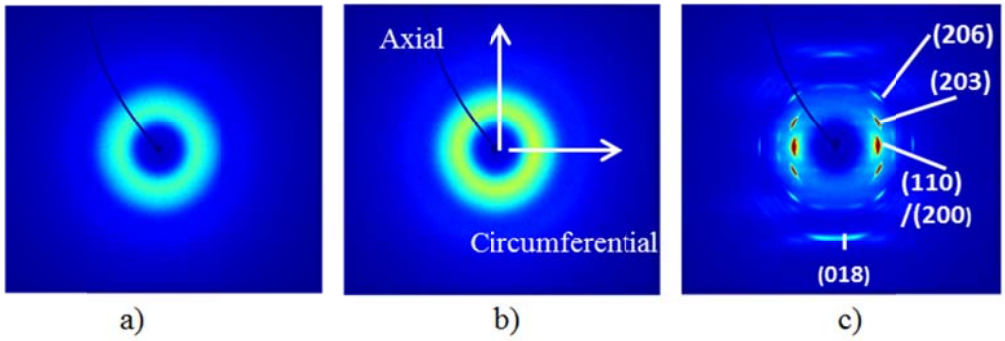

Figure 6 WAXS images of raw material (a), upon heating material to 74°C on the inside (b) and after 96 % axial strain (c).

From the WAXS patterns in Figure 6a it is seen that the raw material showed virtually no crystallinity after tube extrusion (portrayed by a diffuse amorphous halo), as expected. Upon heating, no crystallites are formed, the tube remains low in crystallinity and the material remains isotropic amorphous, which is confirmed by DSC. Figure 6c includes the most reflection planes for strain-induced Poly(L-lactide) (PLLA) and its highly ordered α-crystals, as portrayed by sharp reflections in the (110/200) plane. Uniaxial straining at 74 °C induces crystallinity up to 34 % (c) and is only possible when the strain is nearly 100 %. Strain below this does not induce any notable crystallinity, as axial strain of 24-68 % induced crystallinity of only 2.4 %. As expected, the crystal orientation remains in one direction. However, the orientation is turned 90° compared to the other stretching schemes. The (110)/(200) direction is now parallel to the radial direction rather than the axial direction.

Amorphous vs. crystalline phase.

In Figure 7 the intensity from crystalline phases along with amorphous scattering are shown. Gaussian fitting of each crystalline peak and amorphous scattering was done to investigate differences. X-ray diffraction patterns are identical for both SEQ and SIM biaxial strain, but SEQ biaxial strain peaks are shifted towards lower scattering angles (2θ). Regardless of process route, the SIM and SEQ biaxial strain show the same area under the amorphous phase as well as the crystalline peaks. The amorphous phase decreased with degree of A_{exp} (not shown here) for both SIM and SEQ biaxial strain, which was expected[27] yet the X_c did not increase. This phenomenon could be related to an increase in a transitional phase between the amorphous and the crystalline, before the polymer becomes crystalline. The UNI axially strained tubes did not show the same degree of amorphous diffuse scattering, and therefore the amorphous area is smaller in Figure 7.

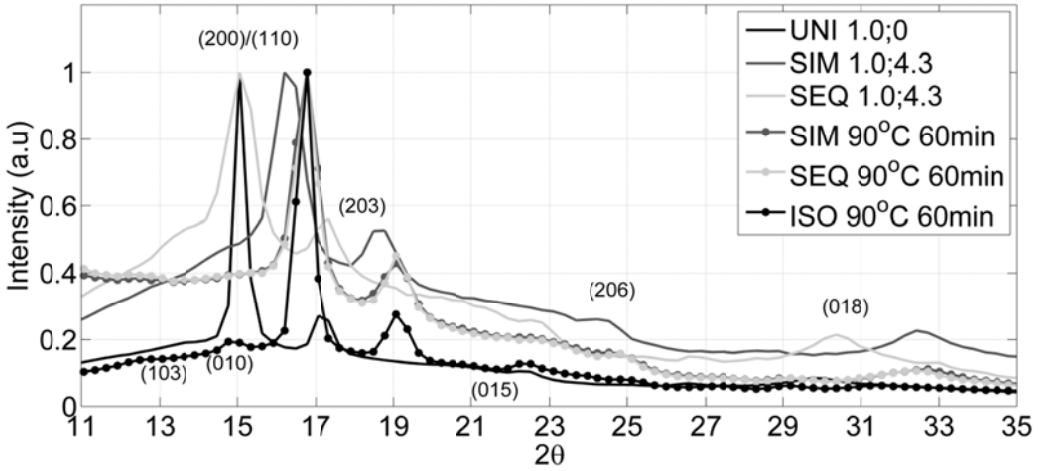

Figure 7 WAXS intensity plot as a function of scattering angle (2θ) and integrated for all azimuthal angles, for UNI at 96 % strain, ISO at 90 °C for 60 min, SIM and SEQ biaxial strain (1.0x4.3) before and after annealing for 60 min at 90 °C and the corresponding crystal planes. [8,18,27,31] Note that the latter two have a large background scattering.

X-ray diffraction peaks occur in multiple planes for the α-crystal phase listed in Table 3, including the planes corresponding to the most commonly occurring reflections for PLLA (103), (010), (110/200), (203), (015) and (207)[27,31]. On the contrary the disordered and less chain-packed α'-crystal phase[31] shows diffraction peaks corresponding to the (110)/(200), (203), (206) and (018) planes at higher 2θ,[27,31] (see Table 3). In this study ISO crystallization shows diffraction peaks solely as α-crystals in (103), (110)/(200), (203), (206) and (015), whereas UNI strain shows peaks at lower 2θ indicating α'-crystals, while lacking the peak for the (103) plane but has the additional (018). The shift in 2θ could be due to the higher crystallization temperature, T_c = 90 °C in ISO crystallization, whereas in UNI strain the T_c = 74 °C. The weak intensity of the (103) reflection is normal for ISO crystallization below 90 °C,[33] and the reflection for the (010) plane is only visible in the ISO crystallization. An additional reflection corresponding to the (015) plane is detected, a reflection not detected for SEQ or SIM biaxial strain.

The difference in 2θ between ISO and strain-induced crystallization was also detected in PLLA films[13]. Stoclet et al, 2010,[13] reported a slightly lower 2θ for UNI strain, explaining that the strain-induced crystals have a larger interplanar spacing. The smaller 2θ means that the crystals have a longer distance between crystal planes than the more stable α-crystal form and possibly a state in which the polymer chains are in a non-equilibrium configuration. Plane (203), (206) and (018) are visible in SIM and SEQ biaxial strain in accordance with reflections of α'-crystals with a larger interplanar spacing. From Figure 7 one can conclude that these reflections are only visible for strain-induced crystallization. Chen et al, 2011,[27] saw a tendency in shift to higher 2θ at higher draw ratios, but this was not detected as given in Table 3**Error! Reference source not found.**. Additionally they discovered the (018) reflection peak after drawing, which is also seen in this study, but more predominant for biaxial strained tubes than UNI strain.

Both SIM and SEQ biaxial strain shows diffraction peaks corresponding to the (110/200) planes at lower 2θ than for the α-crystals in ISO crystallization. The sharp reflection of the (110/200) planes for SEQ biaxial strain is seen at 2θ = 15.1-15.3°, whereas the reflection for SIM is at 16.2-16.5°. This is in agreement with SIM strained PLLA film in a studies by Delpouve et al, 2014,[21] and Hebert et al, 2012,[14] for α'-crystals. For SIM the peak appears at the same 2θ as ISO crystallization, whereas the SEQ biaxial strain peak is closer to the peak in the (110/200) planes for UNI strain. It is likely that it represents the (110)/(200), but is highly disordered. The planes for SIM are detected at angles between 16.2° and 16.5° depending on degree of strain. Due to its similarity with diffraction pattern seen for SEQ, it is likely to represent the α'-crystals and not the α-crystals. The disordered crystal will return to the equilibrium (from α'- to α-crystals) upon annealing for 60 min at 90 °C, which means that further heat processing deletes the processing route history.

The α'-crystals with their looser chain packaging and disordered structure, will according to Saiedlou et al, 2012,[32] result in a lower modulus, and higher elongation at break. SEQ biaxial strain have a larger interplanar spacing than the SIM strained ones, yet there is no difference in their moduli or elongation at break. The crystals for SIM biaxial strain must therefore still be ordered to a degree, where they do not contribute to the stiffness of the material.

Orientation

Figure 8 shows the orientation factor and WAXS images for each SIM and SEQ biaxial strain along with UNI strain, whereas ISO crystallization did not induce crystal orientation. During UNI strain, two intense equatorial diffraction peaks appear transverse to the strain direction, meaning that crystal orientation in the radial direction has been achieved. During transverse strain (eg. SEQ) the diffraction peaks are rotated 90°. It is therefore concluded that a given crystal formation and crystal orientation at the initial UNI strain is rotated 90°, if a radial strain is applied. From the WAXS

analysis, the following structure of the crystals and amorphous chains between crystal regions are portrayed in Figure 9.

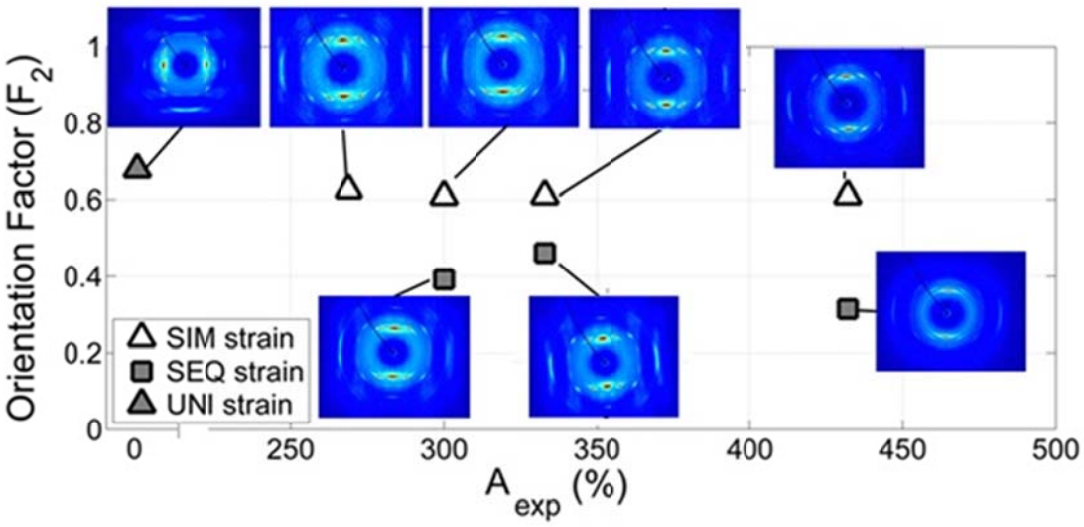

Figure 8 Orientation factor (F_2) for UNI strain, SIM and SEQ biaxially strained tubes as a function of A_{exp}.

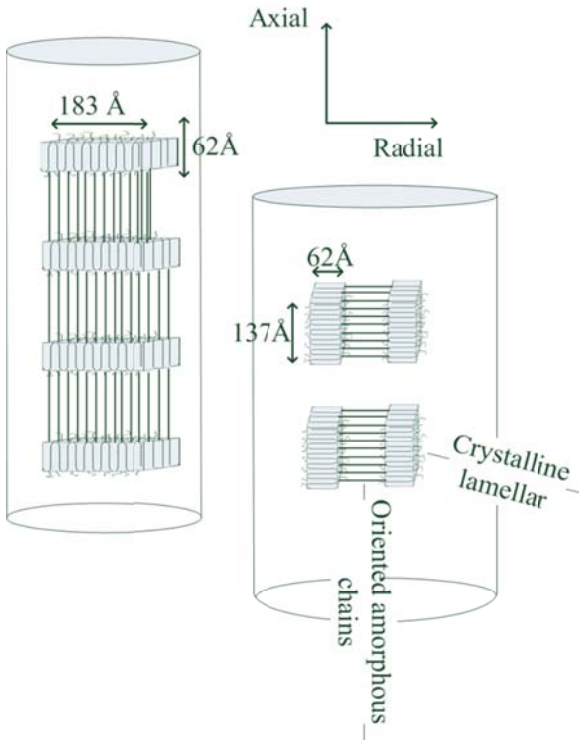

Figure 9 Schematic structural changes of PLLA tubes as they undergo UNI strain (left) and SEQ biaxial straining (right)

The orientation for SIM strain is primarily in axial direction and remains constant as a function of A_{exp}. When increasing the axial strain during SIM (16 %, 44 % and 96 %), the orientation factor and crystallinity remain unaffected. This is not seen during SEQ biaxial strain, where the axial strain influences the final orientation factor. During an axial strain of 96 % the tube has an orientation factor of 0.7 and crystallinity of 34 %, but during the transverse strain the orientation is reduced to 0.4, and becomes lower than observed for SIM with the same degree of axial strain. This means that development of crystals (X_c=34 %) obtained by the axial strain makes it more difficult to achieve orientation radially during the transverse strain and the orientation is reduced further for SEQ biaxial strain (1.0;3.2).

There are two prerequisites for achieving strain-induced crystallization. The first is degree of strain, which must be above 100 % and the second is related to strain rate being equivalent or higher than

chain relaxation time[34]. For all expansion the strain rate remains the same and the lower orientation seen for SEQ biaxial strain (1.0;3.2) could therefore be explained by the degree of strain. A low orientation factor after stretching is usually related to the chains having sufficient time to relax during stretching and would also result in low crystallinity.[25] It is possible that the larger strain in SEQ biaxial strain (1.0;3.2) provides the chains with sufficient relaxation time; however, the crystallinity is not reduced with larger strains. As stated previously the crystallinity remains constant and so does the orientation for SIM, despite larger A_{Total}. However, the orientation decreases for SEQ biaxial strain at high strain as the diffraction peaks become weaker and a more diffuse diffraction ring appears, indicating less anisotropy of the material. It appears that crystals are destroyed upon transverse strain and more predominantly for SEQ biaxial strain than for SIM. As stated previously from Figure 4 these microstructural changes in crystals and the decrease in orientation for SEQ biaxial strain, do not have a negative effect on the mechanical properties.

During annealing, the crystalline orientation is not preserved and is reduced to 0.1 for both SIM and SEQ biaxial strain. It appears that both samples then contain a high number of α-crystals and an interplanar spacing close to that for ISO crystallization. Supposedly annealing will not influence the network achieved during strain, and annealing tends to lock the chain segments in the amorphous phase in such a way that recrystallization becomes unfavourable according to Ou and Camak, 2010,[12]. This is in agreement with the fact that no crystallinity growth was detected for SIM or SEQ biaxially strained samples after post annealing at 90 °C for 60 min. However, the diminishing of the amorphous signal in the WAXS data, when comparing the post annealed sample to the non-annealed, shows that the amorphous phase has changed during the annealing. The crystal orientation factor is reduced to 0.1 for both SEQ and SIM biaxially strained tubes.

In terms of crystal sizes, there is no apparent difference between SIM and SEQ biaxial strain. Zhang et al, 2012,[10] also found crystal sizes at 70-80°C in the range of 60-77 Å in direction of strain,

corresponding to the crystal sizes found in this study in the axial direction after SEQ and SIM biaxial strain and UNI strain. The crystals are larger in the circumferential direction at all expansions, but decrease with A_{exp}. During UNI strain, the crystals are larger in the circumferential direction (see Table 2). Once the radial strain is applied the crystals decrease in the circumferential direction and increase in the axial direction.

It is not known if the crystals formed during axial strain are destroyed once the radial strain is applied, thereby leaving room for new ones to be formed during the expansion. The crystals could also have become distorted by the radial strain and have opposite shape dimensions than the UNI strain crystals. After annealing at 90 °C for 60 min, the SEQ biaxially strained tubes show crystal sizes in the axial direction decrease, whereas crystal sizes in the circumferential direction increase. This could mean that the crystals return to a more relaxed state and shape after annealing. This is less significant for SIM strained tubes.

From Table 1 it is seen that after annealing, the properties for both SEQ and SIM biaxial strain are the same; however, the axial strength is more affected by the annealing, resulting in an even more anisotropic material. Therefore whatever improved mechanical strength and stiffness that is obtained as a result of oriented amorphous chains is lost upon annealing. A slight reduction in crystallinity was detected after annealing, suggesting that some crystals have reduced in size, or disappeared. The loss of stiffness and strength after annealing, cannot be due to a slight reduction in crystallinity, because the gain in mechanical performance as a function of strain, as seen in Figure 4a and b, did not correlate with an increase in crystallinity. It is therefore concluded in this study that mechanical performance of PLLA strained at temperatures above T_g (74 °C) is related to strain-induced chain orientation and packing of crystals, rather than solely related to strain-induced crystallinity.

Conclusion

Crystal formation in PLLA is caused by strain, with uniaxial strain causing the highest degree of crystallinity. The crystal orientation of the normal to the (110/200) plane appears perpendicular to the direction of strain, having a closely packed α'-crystal structure which resembles the α-crystal structure created during isothermal crystallization. Creating a biaxial strain by applying a transverse strain to a uniaxial strain causes a different morphological picture, where crystal orientation and crystallinity is reduced with degree of strain. The sequence of which the biaxial strain occurs furthermore influences the crystal orientation, interplanar spacing, but not the degree of crystallinity. In a stepwise sequential biaxial strain the high degree of crystal orientation formed during uniaxial strain reduces the ability to form highly oriented crystals during the transverse strain, whereas a simultaneous biaxial strain allows formation more aligned crystals, especially at high transverse strains.

In general, applying a transverse strain to an existing uniaxial strain leads to destruction of crystals, while forming new crystals in the transverse direction. A simultaneous biaxial strain, however, where crystals could form and be destroyed simultaneously in each direction of strain, would then contain poorly crystalline regions. It was therefore hypothesized that the sequential biaxial strain would leave the material more anisotropic than the simultaneous biaxial strain. Both straining methods show the same increase in mechanical stiffness and strength as a function of strain, but a different anisotropy, crystal orientation and interplanar spacing. A correlation between the mechanical properties of biaxial strained PLLA and the crystal orientation is therefore not found, but a different isotropy than hypothesized was detected. The simultaneously biaxial strain shows anisotropic properties, with the mechanical properties in the axial direction being the lowest; whereas the transverse strain in the sequential method creates less anisotropic properties at high strains.

From these findings, it was concluded that the mechanical performance of PLLA strained at temperature above T_g (74 °C) is related to strain-induced orientation of the chains in the amorphous region, rather than solely related to strain-induced crystallinity and orientation.

References:

1 Nair LS and Laurencin CT, *Prog. Polym. Sci.* **32:** 762-798 (2007).

2 Stoclet G, Séguéla R, Lefebvre JM, Li S and Vert M, *Macromolecules* **44:**, 4961-4969 (2011).

3 Lim LT, Auras R and Rubino M, *Prog. Polym. Sci.* **33:** 820–852 (2008).

4 Lasprilla AJR, Martìnez GAR, Lunelli BH, Jardini AL and Filho RM, *Biotechnology Advances* **30:** 321-328 (2012).

5 Nampoothiri KM, Nair NR and John RP, *Bioresour. Technol*. **101:** 8493–8501 (2010).

6 Takahashi K, Sawai D, Yokoyama T, Kanamoto T and Hyon S, *Polymer* **45:** 4969-4976 (2004).

7 Zhang J, Duan Y, Sato H, Tsuji H, Noda I, Yan S and Ozaki Y, *Macromolecules* **38:** 8012-8021 (2005)

8 Cocca M, Lorenzo M, Malinconico M and Frezza V, *Eur. Polym J.* **47:** 1073-1080 (2011).

9 Carrasco F, Pagès P, Gámez-Péres J, Santana OO and Maspoch ML, *Polym. Degrad. Stab.***95:** 116-125 (2010)

10 Zhang X, Schneider K, Liu G, Chen J, Brüning K, Wang D and Stamm M, *Polymer* **53:** 648–656 (2012).

11 Ou X and Cakmak M, *Polym* **49:** 5344–5352 (2008).

12 Ou X and Cakmak M, *Polym* **51:** 783–792 (2010).

13 Stoclet G, Séguéla R, Lefebvre JM, Elkoun S and Vanmansart C, *Macromolecules* **43:** 1488–1498 (2010).

14 Hebért J, Wood-Adams P, Heuzey M, Dubois C and Brisson J, *J. Polym. Sci., Part B: Polym. Phys.* **51:** 430-440 (2012)

15 Lee SC, Han JI and Heo JW, *Polymer* **54:** 3624-3632 (2013).

16 Løvdal ALVL, Laursen LL , Andersen TL, Madsen B and Mikkelsen LP, *J. Appl. Polym. Sci* **128:** 203-2045 (2013)

17 Velazquez-Infante JC, Gámez-Péres J, Franco-Urquiza EA, Santana OO, Carrasco F and Maspoch ML, *J. Appl. Polym. Sci.* **127:** 2661-2669 (2013)

18 Oh MO and Kim SH, *Polym Int* **63:** 1247-1253 (2013).

19 Xiong Z, Liu G, Zhang X, Wen T, Vos S, Joziasse C and Wang D, *Polymer* **54:** 964-971 (2013).

20 Stoclet G, Séguéla R, Vanmansart C, Rochas C and Lefebvre JM, *Polymers* **53:** 519-528 (2012).

21 Delpouve N, Delbreilh L, Stoclet G, Saiter A and Dargent E, *Macromolecules* **47:** 5186-5197 (2014).

22 Tsai C, Wu R, Cheng H, Li S, Siao Y, Kong D and Jang G, *Polym. Degrad. Stab.* **95:** 1292-1298 (2010).

23 Wu J, Yen M, Wu C, Li C and Kuo MC, *J Polym Environ* **21:** 303-311 (2013).

24 Apitz D, Bertram RP, Benter N, Hieringer W, Andreasen JW, Nielsen MM, Johansen PM and Buse K, *Phys. Rev. E* **72:** 036610-1-036610-10 (2005).

25 Sakurai S, Aida S, Okamoto S, Ono T, Imaizumi K and Nomura, S, *Macromolecules* **34:** 3672-3678 (2001).

26 Zhang X, Schneider K, Liu G, Chen J, Brüning K, Wang D and Stamm M, *Polymer* **52:** 4141-4149 (2011).

27 Chen X, Kalish J and Hsu SL, J. *Polym. Sci., Part B: Polym. Phys.* **49:** 1446–1454 (2011)

28 B. Wunderlich, Thermal Analysis, Academic Press, 1990, pp. 417-431

29 Weir NA, Buchanan FJ, Orr JF and Farrar DF, *Biomaterials* **25:** 3939-3949 (2004).

30 Tsuji H and Ikada Y, *Polymer* **36:** 2709-2716 (1995).

31 Wang Y, Funari SS and Mano JF, *Macromol. Chem. Phys.* **207:** 1262-1271 (2006).

32 Saeidlou A, Huneault MA, Li H and Park CB, *Prog. Polym. Sci.* **37:** (2012), 1657-1677

33 Kawai T, Rahman N, Matsuba G, Nishida K, Kanaya T, Nakano M, Okamoto H, Kawada J, Usuki A, Honma N, Nakajima K and Matsuda M, *Macromolecules* **2007,** *40,* 9463-9469

34 Mahendrasingam A, Blundell DJ, Parton M, Wright AK, Rasburn J, Narayanan T and Fuller W *Polymer* **46:** 6009-6015 (2005).

Table 1. Elastic modulus (E), yield stress (σ_y), maximal stress (σ_{max}) for circumferential (circ) and axial directions. Statistical significance difference (level of 5 %) between one A_{exp} to another is denoted by either [a] showing significance difference from (0.5;2.6), and [b] showing significance difference between SIM and SEQ biaxial strain for the same A_{exp}.

	(ε_a; ε_r)	**$E_{20\text{-}40\ (circ)}$ (MPa)**	**$\sigma_{y\ (circ)}$ (MPa)**	**$\sigma_{max\ (circ)}$ (MPa)**	**$E_{20\text{-}40\ (axial)}$ (MPa)**	**$\sigma_{y\ (axial)}$ (MPa)**
SIM	(0.2;2.6)	3274±198	77±2	119±10	2320±273	67±7
SIM	(0.5;2.6)	3456±195	78±2	119±8	2614±219[b]	76±6[b]
SIM	(0.2;3.3)	3834±292 [a]	86±3 [a]	131±10 [a,b]	2983±174[b]	80±6[b]
SIM	(1.0;3.2)	3997±255 [a]	87±3 [a]	137±9 [a,b]	2848±189 [a,b]	77±3 [a,b]
SIM (90°C)	(1.0;3.2)	2963±338	78±5	140±12	1961±196	67±3
SEQ	(0.5;2.6)	3460±258	82±5	128±13	2983±174[b]	80±6
SEQ	(0.2;3.3)	3946±321 [a]	89±4 [a]	144±13 [a,b]	3197±143 [a,b]	86±5[b]
SEQ	(1.0;3.2)	3964±283 [a]	91±4 [a]	150±9 [a,b]	3966±275 [a,b]	102±3 [a,b]
SEQ(90°C)	(1.0;3.2)	2821±217	77±3	136±13	2028±196	83±11

Table 2. Crystallinity (X_c) from DSC and crystallite sizes from XRD for circumferential (D_c) and axial direction (D_a).

	(ε_a; ε_r)	**Xc (%)**	**T_g (°C)**	**(D_c) (Å)**	**(D_a) (Å)**
As extruded	(0)	1	62	-	-
SIM	(0.2;2.6)	30	62	67	160
SIM	(0.5;2.6)	32	63	70	151
SIM	(0.2;3.3)	29	66	69	139
SIM	(1.0;3.2)	31	65	65	137
SIM(90°C)	(1.0;3.2)	28	65	65	141
SEQ	(0.5;2.6)	29	64	63	160
SEQ	(0.2;3.3)	30	65	63	146
SEQ	(1.0;3.2)	32	65	60	129
SEQ(90°C)	(0.5;2.6)	30	65	45	142
UNI	(1.0;0)	34	61	183	62
UNI (120°C)	(1.0;0)	36	60	160	126
ISO (90 °C)	(0)	29	61	62	136

Table 1. Scattering angles (2θ) and their crystal planes for PLLA after ISO crystallization, UNI axial, SIM and SEQ biaxial strain before and after annealing. For comparison the scattering angles for α and α'-crystals.[26,30]

	(ε_a; ε_r)	(103) **2θ(°)**	(010) **2θ(°)**	(110/200) **2θ(°)**	(203) **2θ(°)**	(015) **2θ(°)**	(206) **2θ(°)**	(018) **2θ(°)**
SIM	0.5;3.0			16.5	19.1		24.8	33.0
SIM	0.2:4.3			16.5	18.7		24.5	32.7
SIM	1.0;4.3			16.2	18.8		24.3	32.4
SIM (90°C 60min)								32.72
SEQ	0.5;3.0			15.1	17.3		22.8	30.4
SEQ	0.2;4.3			15.3	17.3		22.8	30.4
SEQ	1.0;4.3			15.1	17.3		22.8	30.4
SEQ (90°C 60min)								32.4
UNI	1.0;0			15.2	17.1		22.5	
ISO		12.5	14.8	16.8	19.1	22.2		
α[26,30]		12.6	14.8-15.0	16.7	19.1	22.2		
α'[26,30]				16.6	18.9		24.7	33.1